Methods and Applications

Adaptive Fourier Decomposition of the First Three SARS-CoV-2 Infection Waves with Epidemic Intervention — London, UK, 2020–2022

Zige Liu[1]; Guibin Lu[1]; Cheokieng Vong[2]; Zhiqi Zeng[3,4,5]; Wei He[1]; Zhijie Lin[1]; Cuiyun Lin[6]; Kaichin Hsieh[7]; Zifeng Yang[3,5,8]; Arlindo L. Oliveira[4,9,10]; Chitin Hon[1,4,5,8,#]

ABSTRACT

Background: This study provides a detailed analysis of the daily fluctuations in coronavirus disease 2019 (COVID-19) case numbers in London from January 31, 2020 to February 24, 2022. The primary objective was to enhance understanding of the interactions among government pandemic responses, viral mutations, and the subsequent changes in COVID-19 case incidences.

Methods: We employed the adaptive Fourier decomposition (AFD) method to analyze diurnal changes and further segmented the AFD into novel multi-component groups consisting of one to three elements. These restructured components were rigorously evaluated using Pearson correlation, and their effectiveness was compared with other signal analysis techniques. This study introduced a novel approach to differentiate individual components across various time-frequency scales using basis decomposition methods.

Results: Analysis of London's daily COVID-19 data using AFD revealed a strong correlation between the "stay at home" directive and high-frequency components during the first epidemic wave. This indicates the need for sustained implementation of vaccination policies to maintain their effectiveness.

Discussion: The AFD component method provides a comprehensive analysis of the immediate and prolonged impact of governmental policies on the spread of severe acute respiratory syndrome coronavirus 2 (SARS-CoV-2). This robust tool has proven invaluable for analyzing COVID-19 pandemic data, offering critical insights that guide the formulation of future preventive and public health strategies.

Since December 2019, the global spread of severe acute respiratory syndrome coronavirus 2 (SARS-CoV-2) has placed unprecedented strain on healthcare systems and significantly disrupted daily life (*1–4*). London has experienced three major epidemic waves from January 2020 to April 2021, each characterized by the dominance of different SARS-CoV-2 variants that emerged through successive mutations, specifically Alpha (B.1.1.7), Delta (B.1.617), and Omicron (B.1.1.529). Notably, due to extensive vaccination efforts and the reduced severity of the Omicron variant, the third wave resulted in fewer hospitalizations compared to previous waves. Therefore, a comprehensive analysis of daily coronavirus disease 2019 (COVID-19) trends in London is essential to understand transmission patterns, assist policymakers in developing prevention strategies, and improve public health outcomes and awareness (*5–6*).

Epidemiological modeling research aimed at examining variations in COVID-19 case numbers encounters challenges frequently due to the non-linear complexity of pandemic-related data, as discussed by Stanovov et al. (*7*). In an attempt to manage this complexity, Huang et al. and Dong et al. utilized the empirical mode decomposition (EMD) method to effectively break down non-linear data into identifiable components. However, this method lacks a solid mathematical foundation (*8–9*). In contrast, the variational mode decomposition (VMD) method, employed by Saadaoui et al., provides an alternative but struggles to separate signal components that are indistinct in the Fourier spectrum (*10*). To surpass these limitations, Qian et al. (*11–13*) have developed the adaptive Fourier decomposition (AFD), which offers a robust mathematical structure and improved adaptation to the signal wave curve, facilitating a more precise analysis of COVID-19 case fluctuations (Supplementary Material, available at https://weekly.chinacdc.cn/).

In this study, we employed the AFD method to analyze daily COVID-19 infection trends in London. AFD's advanced time-frequency models effectively address scale aliasing issues, allowing for accurate measurement of trends' direction and velocity. The AFD model, through signal decomposition into distinct components, successfully pinpointed significant peaks during the study period. Furthermore, we conducted a comparative analysis using EMD and VMD methods to enhance the robustness of our findings.

METHODS

New Construction Components Based on AFD Results

There are a few different types of AFD, including core AFD, cyclic AFD, and unwinding AFD, which are broadly used in numerous fields (*14–23*). We proposed a novel optimization algorithm (Equation 1), viewed as an addition to the core AFD method. To secure sufficient decomposition results for large-scale data, extra layers of decompositions are processed. However, the generation of superfluous data is unavoidable. Therefore, by using the new component constructing strategy and merging partially decomposed components, the accuracy and reliability of the data can be improved, no matter how large or small the frequency signals are. As a result, we constructed new components based on the decomposition results (*13*):

$$D_p(q) = \sum_{m=pq-q+1}^{pq} C_m B_m(z),\qquad(1)$$

$$where\, z = e^{jt},$$

$$C_m = \langle F_m, e_{\{a_m\}} \rangle,$$

$$and\ B_m(z) = \frac{\sqrt{1-|a_m|^2}}{1-\bar{a}_m z} \prod_{k=1}^{m-1} \frac{z-a_k}{1-\bar{a}_k z}.$$

The original signal was obtained by constructing all of the components (Equation 2).

$$W_q = \sum_{p=1}^{r} D_p(q)\qquad(2)$$

Sample and Data

In this study, we conducted a detailed analysis of the daily fluctuations in COVID-19 case counts in London from January 31, 2020, the date of the first confirmed case, to February 24, 2022 (Figure 1), when the Prime Minister announced the removal of all legal restrictions related to SARS-CoV-2.

RESULTS

Enhanced Construction Components Using Results from AFD

Figure 2 illustrates a method for constructing new components using the AFD algorithm, as outlined in the Supplementary Method. The process involves analyzing London's daily COVID-19 case count data with the AFD algorithm to discern the number of infection cases at different time-frequency scales. This enhanced method merges partially decomposed components, improving data reliability. Figure 3 displays the first to eighth vertical lines representing the frequency components from lowest to highest. These lines indicate shifts in the number of infections at various scales, transitioning from long-term to short-term changes. The horizontal lines labeled a, b, and c represent the construction methods for one to three
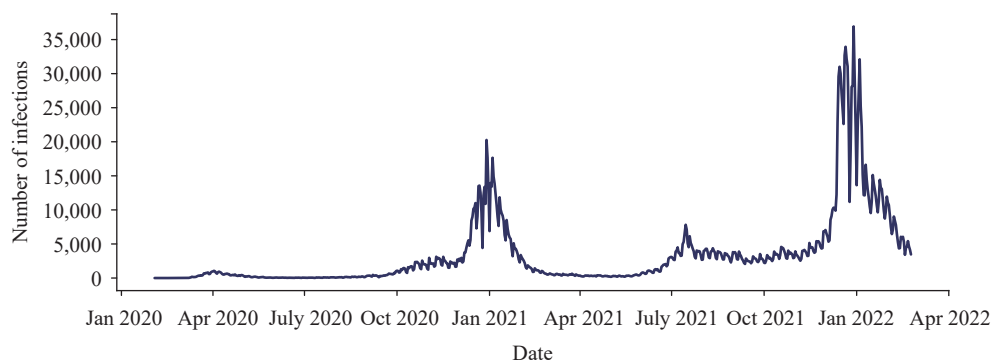

FIGURE 1. Daily COVID-19 infections in London from January 31, 2020 to February 24, 2022.
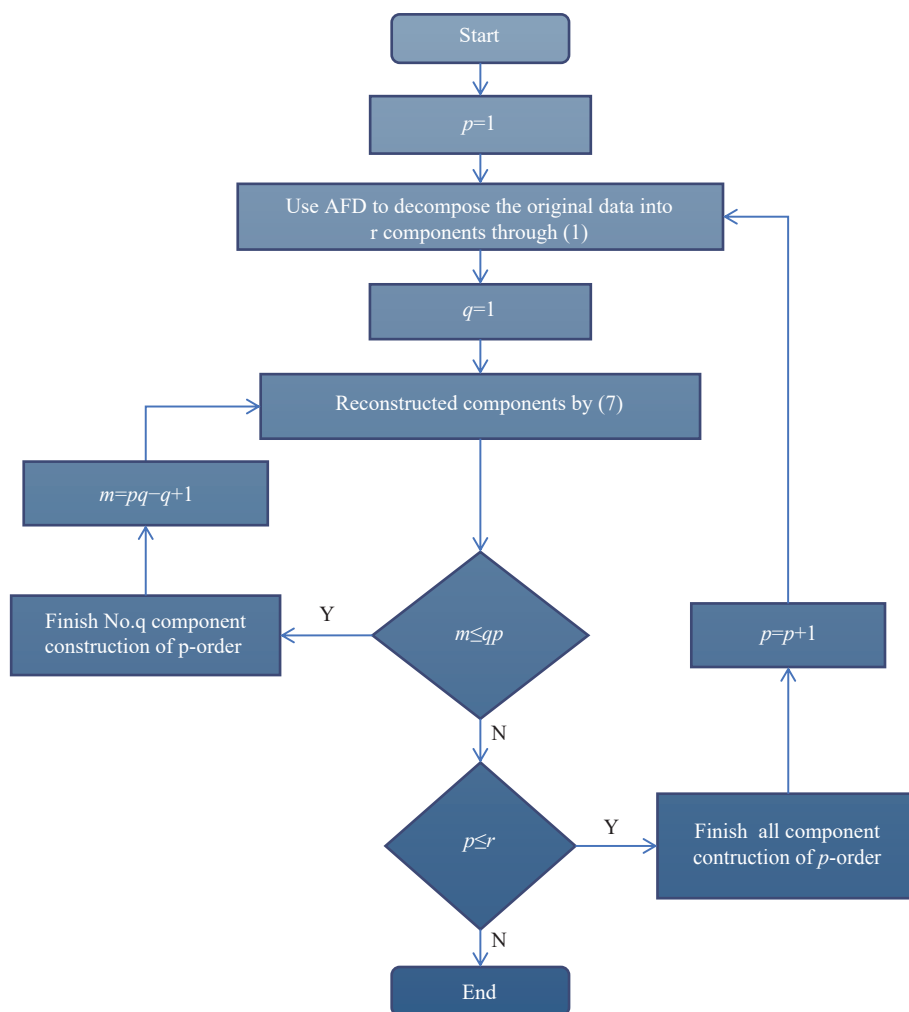Abbreviation: COVID-19=coronavirus disease 2019.

FIGURE 2. Construction of a new component flowchart for AFD.
Abbreviation: AFD=adaptive Fourier decomposition.

components, respectively, as detailed in Equation 1. These lines demonstrate variations in daily COVID-19 infection counts under different epidemic prevention policies during various AFD construction stages.

Components Extracted Using the AFD Method

The results depicted in Figure 3 indicate that the primary components of the enhanced construction follow a trend similar to the daily infection counts in London during the analysis period (Table 2). Notably, the elevated vaccination rates played a crucial role in establishing herd immunity, effectively protecting against the variant.

From the third to the sixth components, there were notable frequency peaks during the third wave, leading to significant increases and decreases in COVID-19 cases around December 2021. This pattern is linked to

the relaxation of preventive measures, such as allowing household mixing, marking the beginning of a phased lockdown exit. In contrast, the seventh and eighth components showed marked fluctuations starting in 2020, with minor peaks during the first wave and more pronounced oscillations observed during the second and third waves. These trends suggest that these waves were captured at a relatively high frequency, likely due to early policies aimed at reducing social contact, which were critical in controlling the transmission of SARS-CoV-2 in London.

Construction Components Derived from AFD

Figure 3 presents a horizontal arrangement of results from the AFD-based, AFD-second, and AFD-third new construction components. The interrelations between results from various new construction
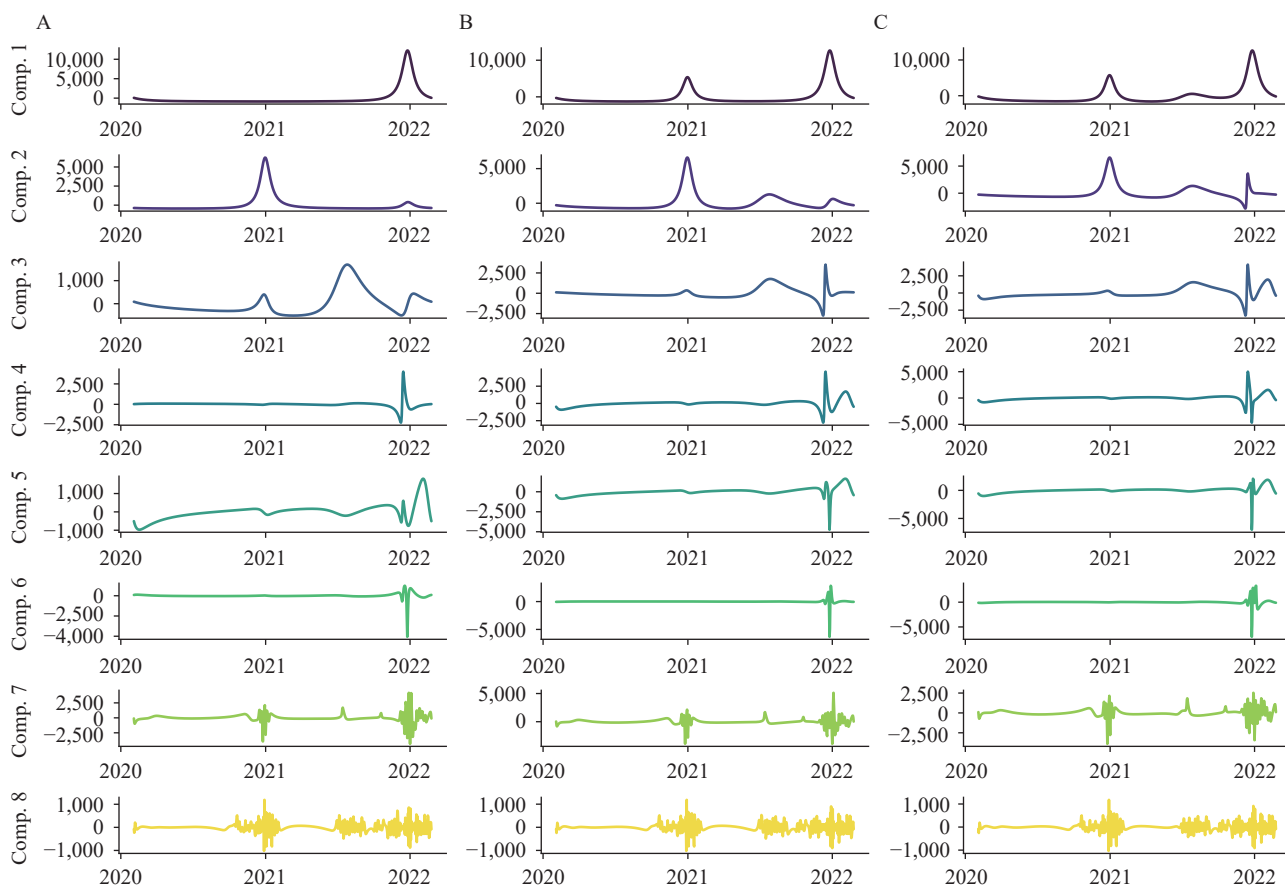
FIGURE 3. Various new construction components based on AFD. (A) AFD-based decompositions; (B) AFD-second decompositions; (C) AFD-third decompositions.
Abbreviation: AFD=adaptive Fourier decomposition.

TABLE 1. Identified waves and corresponding control policies.

Wave	Start time	End time	Main issues	Government policy
1st	Jan 31, 2020	Sep 6, 2020	The rapid increase in alpha variant spreading across London. Limited COVID-19 testing was available, therefore the number of confirmed cases was underestimated.	The first national lockdown included a "stay at home" strategy, no mixing of households, closure of all shops selling non-essential goods and stopping all social events.
2nd	Sep 7, 2020	Apr 12, 2021	The rapid rise in infections is attributed to the rapid spread of new delta variants causing high morbidity and mortality rates.	The second national lockdown included staying in household bubbles, leisure and entertainment venues must be closed. Schools remained open. The third national lockdown includes leisure and entertainment that were still shut. However, meeting support bubbles and exercising with the household were allowed. Schools moved to remote learning.
3rd	Jul 1, 2021	Feb 24, 2022	Although the Omicron variant pushed the prevalence of the virus to unprecedented levels, the vaccine built up immunity, sustained protection against severe disease in the population and reduced severity of the Omicron variant.	England began a phased exit from lockdown, Prime Minister announced all remaining domestic restrictions in law were removed.

components were further analyzed, as detailed in Table 2. Notably, improvements in the first and second order components were evident in the third-order new construction components, leading to a more precise depiction of daily infection rates. The first-order component from the third order displayed a notably higher coefficient value (0.955) compared to the other seven components, highlighting its superior

TABLE 2. Correlations between new construction components and original infections.

Wave	Correlations (*P* value) between components and original methods			Correlations (*P* value) between components of distinct methods		
	AFD-based	AFD-second	AFD-third	AFD-based& AFD-second	AFD-based& AFD-third	AFD-second& AFD-third
Comp. 1	0.834*	0.926*	0.945*	0.900*	0.980*	0.882*
	(0.000)	(0.000)	(0.000)	(0.000)	(0.000)	(0.000)
Comp. 2	0.403*	0.445*	0.468*	0.907*	0.950*	0.862*
	(0.000)	(0.000)	(0.000)	(0.000)	(0.000)	(0.000)
Comp. 3	0.187*	0.237*	0.281*	0.787*	0.843*	0.664*
	(0.000)	(0.000)	(0.000)	(0.000)	(0.000)	(0.000)
Comp. 4	0.146*	0.211*	0.230*	0.694*	0.917*	0.637*
	(0.000)	(0.000)	(0.000)	(0.000)	(0.000)	(0.000)
Comp. 5	0.152*	0.177*	0.200*	0.856*	0.884*	0.757*
	(0.000)	(0.000)	(0.000)	(0.000)	(0.000)	(0.000)
Comp. 6	0.091*	0.131*	0.160*	0.698*	0.817*	0.571*
	(0.000)	(0.000)	(0.000)	(0.000)	(0.000)	(0.000)
Comp. 7	0.221*	0.200*	0.178*	0.904*	0.886*	0.800*
	(0.000)	(0.000)	(0.000)	(0.000)	(0.000)	(0.000)
Comp. 8	0.065*	0.064*	0.062*	0.981*	0.980*	0.961*
	(0.000)	(0.000)	(0.000)	(0.000)	(0.000)	(0.000)

Note: All correlation coefficients were estimated using Pearson's correlation method.
Abbreviation: AFD=adaptive Fourier decomposition.
* indicates that the correlation coefficient is statistically significant (*P*<0.001).

efficacy. Additionally, Table 2 emphasizes the significance of lower-frequency components in depicting the overall trend of the pandemic.

Next, we analyzed the third-order decomposition results utilizing the AFD method and compared these with the results from two other widely used time-frequency methods, EMD and VMD. Figure 4 illustrates the decomposition results for EMD and VMD in columns b and c, respectively. Furthermore, Table 3 displays the correlations between the components of each method and the initial COVID-19 infection counts, as established via Pearson correlation analysis (Supplementary Material) (*21*).

By calculating the Pearson correlation across components isolated by these three techniques, we further established that the AFD method outperforms others in extracting vital details about the effectiveness of government control policies. This analysis solidifies the AFD method as the most effective among the assessed methodologies in capturing relevant data.

Linking AFD to Government Policies

In this research, findings from the third-order AFD construction for new components were integrated with daily COVID-19 infection counts to analyze the impact of epidemic prevention policies. The analysis was framed using the timeline of London's three-wave epidemic, resulting in the division of the data into three segmented graphs (Figure 5). Notably, the components illustrated in these figures demonstrate correlation coefficients exceeding 0.7, falling within a 5% confidence interval (*CI*). Figure 5A illustrates the initial response to the epidemic in London. The seventh component in this figure indicates that the "delayed phase" policies preemptively mitigated the impact of this wave, effectively suppressing the spread of SARS-CoV-2 and curtailing the progression of the epidemic. Additionally, other policies implemented during the first wave, including various cancellations and disease containment measures, contributed to the gradual control of SARS-CoV-2 infections.

Figure 5B depicts that starting in September 2020, London encountered a second epidemic wave, resulting in a second national lockdown. The first and second components of the AFD analysis from this period indicate that this policy effectively mitigated the
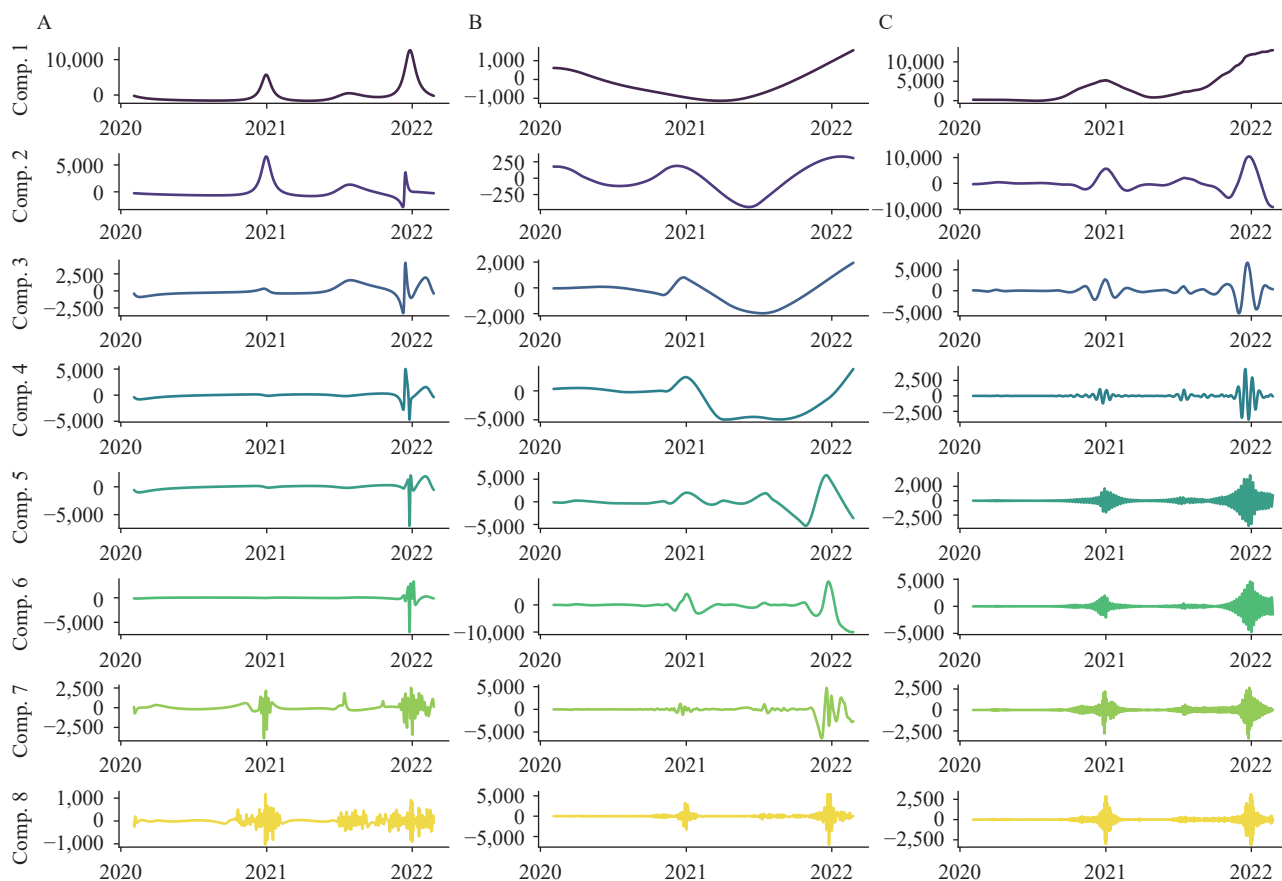
FIGURE 4. Decompositions based on AFD-third, EMD, and VMD. (A) AFD-third decompositions; (B) EMD-based decompositions; (C) VMD-based decompositions.
Abbreviation: AFD=adaptive Fourier decomposition; EMD=empirical mode decomposition; VMD=variational mode decomposition.

epidemic's impact, leading to a rapid decrease in daily COVID-19 infection counts. The effects of the second national lockdown were not immediate but became evident over time.

Figure 5C illustrates that despite the Omicron variant elevating the prevalence of SARS-CoV-2 to unprecedented levels, widespread vaccination efforts conferred both individual and herd immunity, providing sustained protection against severe disease in the population. The policies implemented during the third wave of the epidemic correlated with the primary component of the AFD results, suggesting that the impact of the two-dose vaccination policy on controlling the epidemic was moderate and underscores the necessity for its prolonged and continuous implementation.

DISCUSSION

Herein, we present a detailed analysis of daily variations in COVID-19 cases in London from January 31, 2020 to February 24, 2022. We compared the AFD method with the EMD and VMD methods to establish a clearer mathematical framework for such analyses (22–24).

Our findings indicated that the AFD variant algorithm proposed by Qian et al. does not fully correspond with the specific COVID-19 data from London (14–17). By reconfiguring components of the AFD, new combinations were developed (Figure 3B–3C), which surpassed the efficacy of the basic AFD model by Qian et al. (Figure 3A) (11–12,18–20).

The AFD variant algorithm was utilized to analyze the daily COVID-19 case numbers, facilitating a comprehensive examination of the epidemic's spread dynamics. This method indicated that low-frequency components corresponded with the outbreak and declining phases of the epidemic, reflecting the long-term impacts of policies designed to mitigate SARS-

TABLE 3. Correlations between components of different methods and original infections.

Wave	Correlations (*P* value) between components and original methods			Correlations (*P* value) between components of distinct methods		
	AFD-third	EMD-based	VMD-based	AFD-third& EMD-based	AFD-third& VMD-based	EMD-based& VMD-based
Comp. 1	0.945*	0.503*	0.735*	0.517*	0.710*	0.675*
	(0.000)	(0.000)	(0.000)	(0.000)	(0.000)	(0.000)
Comp. 2	0.468*	0.389*	0.640*	0.115*	0.466*	0.096*
	(0.000)	(0.000)	(0.000)	(0.000)	(0.000)	(0.000)
Comp. 3	0.281*	0.142*	0.348*	−0.251	0.230*	0.027*
	(0.000)	(0.000)	(0.000)	(0.000)	(0.000)	(0.000)
Comp. 4	0.230*	0.575*	0.151*	−0.145	0.598*	0.008
	(0.000)	(0.000)	(0.000)	(0.000)	(0.000)	(−0.231)
Comp. 5	0.200*	0.229*	0.182*	−0.441	0.259*	0.004
	(0.000)	(0.000)	(0.000)	(0.000)	(0.000)	(−0.525)
Comp. 6	0.160*	0.045	0.182*	0.239*	0.421*	0.001
	(0.000)	(−0.219)	(0.000)	(0.000)	(0.000)	(−0.933)
Comp. 7	0.178*	0.193*	0.089**	0.434*	0.201*	0.008
	(0.000)	(0.000)	(−0.014)	(0.000)	(0.000)	(−0.242)
Comp. 8	0.062*	0.259*	0.059	0.240*	0.364*	0.228*
	(0.000)	(0.000)	(−0.107)	(0.000)	(0.000)	(0.000)

Note: All correlation coefficients were estimated using Pearson's correlation method.
Abbreviation: AFD=adaptive Fourier decomposition; EMD=empirical mode decomposition; VMD=variational mode decomposition.
* indicates that the correlation coefficient is statistically significant (*P*<0.001).

CoV-2 transmission. Conversely, high-frequency components appeared to reflect the effects of short-term policies and variations due to stochastic factors.

During the SARS-CoV-2 pandemic, requires swift policy responses, but this urgency can lead to insufficient research and justification, resulting in blindness and instability. As the pandemic evolves, cities may need to adjust policies to adapt, but due to the time and procedures involved, policy adjustments may lag behind.

Therefore, we developed a novel method to monitor and assess the effectiveness of policies in London, one of the cities most severely affected globally. This approach tackles the challenge of uniformly measuring the timing of implementation and termination of epidemic prevention policies through quantitative evaluation indicators.

The use of the AFD method provides valuable perspectives on the immediate and prolonged impacts of interventions aimed at curbing the spread of SARS-CoV-2. It has proven to be an effective analytical tool for investigating COVID-19 pandemic data, and it offers crucial insights for shaping future preventive and public health strategies.

Corresponding author: Chitin Hon, cthon@must.edu.mo.

1 Department of Engineering Science, Faculty of Innovation Engineering, Macau University of Science and Technology, Macau SAR, China; 2 Queen Ethelburga's Collegiate, Thorpe Underwood Estate, York, UK; 3 State Key Laboratory of Respiratory Disease, National Clinical Research Center for Respiratory Disease, Guangzhou Institute of Respiratory Health, The First Affiliated Hospital of Guangzhou Medical University, Guangzhou City, Guangdong Province, China; 4 Respiratory Disease AI Laboratory on Epidemic and Medical Big Data Instrument Applications, Department of Engineering Science, Faculty of Innovation Engineering, Macau University of Science and Technology, Macau SAR, China; 5 Guangzhou Key Laboratory for Clinical Rapid Diagnosis and Early Warning of Infectious Diseases, KingMed School of Laboratory Medicine, Guangzhou Medical University, Guangzhou City, Guangdong Province, China; 6 Faculty of Innovation Engineering, School of Computer Science and Engineering, Macau University of Science and Technology, Macau SAR, China; 7 University College London, UCL Faculty of Engineering Sciences, London, UK;
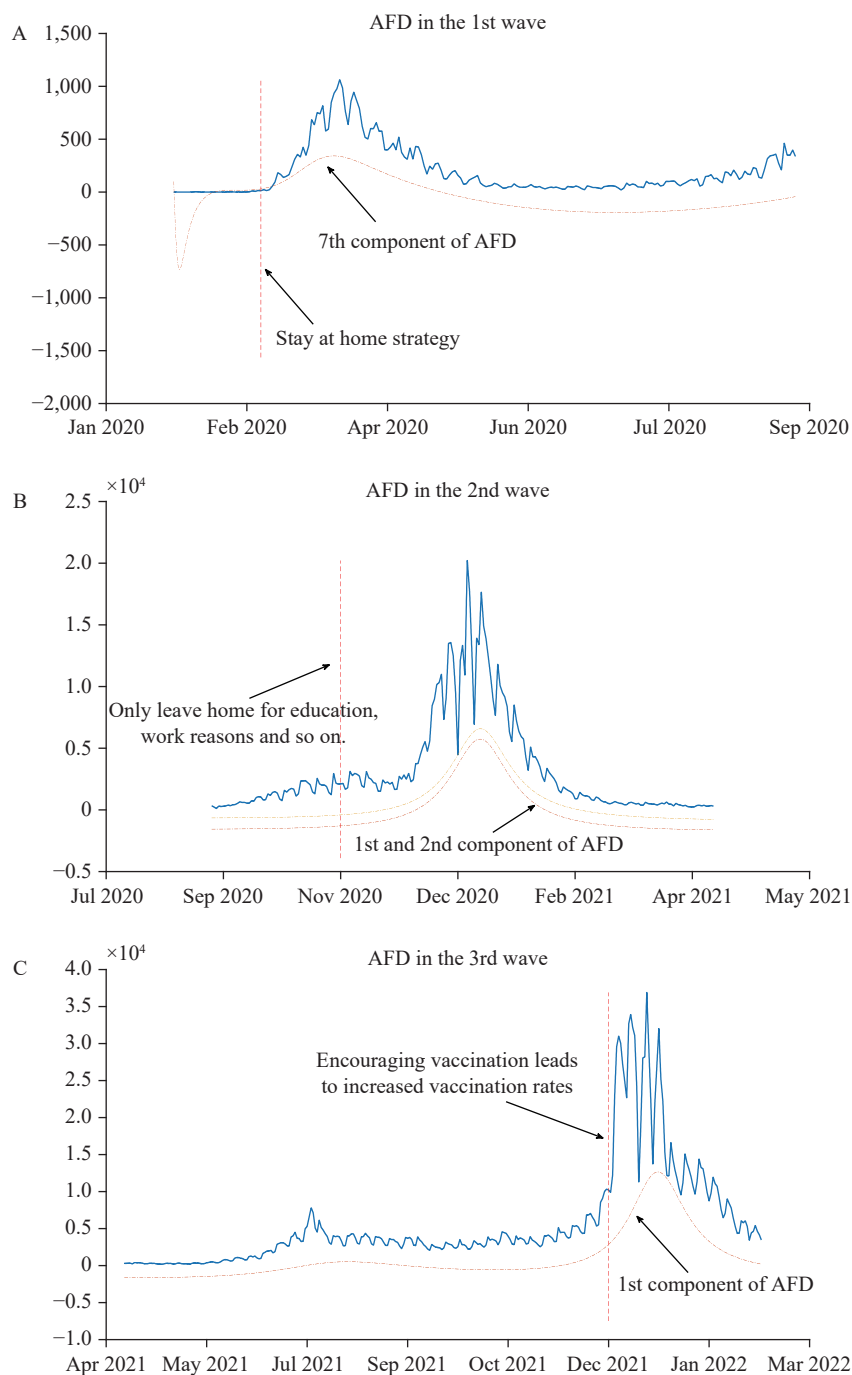
FIGURE 5. AFD components. (A) During the first wave; (B) during the second wave; (C) during the third wave.
Abbreviation: AFD=adaptive Fourier decomposition.

[8] Guangzhou Laboratory, Guangzhou City, Guangdong Province, China; [9] Instituto de Engenharia de Sistemas e Computadores: Investigação e Desenvolvimento em Lisboa, Lisboa, Portugal; [10] Instituto Superior Técnico, Universidade de Lisboa, Lisboa, Portugal.

REFERENCES

1. WHO. WHO director-general's opening remarks at the media briefing on COVID-19 - 11 March 2020. World Health Organization. 2020. https://www.who.int/director-general/speeches/detail/who-director-general-s-opening-remarks-at-the-media-briefing-on-covid-19---11-march-2020. [2020-3-11].

2. Liang JY, Liu RB, He W, Zeng ZQ, Wang YQX, Wang BY, et al. Infection rates of 70% of the population observed within 3 weeks after release of COVID-19 restrictions in Macao, China. J Infect 2023;86(4): 402 – 4. https://doi.org/10.1016/j.jinf.2023.01.029.

3. Zeng ZQ, Qu W, Liu RB, Guan WD, Liang JY, Lin ZJ, et al. Real-time assessment of COVID-19 epidemic in Guangdong Province, China using mathematical models. J Thorac Dis 2023;15(3):1517 – 22.

https://doi.org/10.21037/jtd-23-47.

4. Zhou MZ, Kan MY. The varying impacts of COVID-19 and its related measures in the UK: A year in review. PLoS One 2021;16(9):e0257286. https://doi.org/10.1371/journal.pone.0257286.

5. Elliott P, Bodinier B, Eales O, Wang HW, Haw D, Elliott J, et al. Rapid increase in omicron infections in england during december 2021: REACT-1 study. Science 2022;375(6587):1406 – 11. https://doi.org/10.1126/science.abn8347.

6. Kirsebom FCM, Andrews N, Stowe J, Toffa S, Sachdeva R, Gallagher E, et al. COVID-19 vaccine effectiveness against the omicron (BA. 2) variant in England. Lancet Infect Dis 2022;22(7):931 – 3. https://doi.org/10.1016/S1473-3099(22)00309-7.

7. Okabe Y, Shudo A. Microscopic numerical simulations of epidemic models on networks. Mathematics 2021;9(9):932. https://doi.org/10.3390/math9090932.

8. Huang AQ, Liu XJ, Rao CR, Zhang Y, He YF. A new container throughput forecasting paradigm under COVID-19. Sustainability, 2022;14(5):2990. https://doi.org/10.3390/su14052990.

9. Dong R, Ni SW, Ikuno S. Nonlinear frequency analysis of COVID-19 spread in Tokyo using empirical mode decomposition. Sci Rep 2022;12 (1):2175. https://doi.org/10.1038/s41598-022-06095-w.

10. Saâdaoui F, Mefteh-Wali S, Ben Jabeur S. Multiresolutional statistical machine learning for testing interdependence of power markets: a Variational Mode Decomposition-based approach. Expert Syst Appl 2022;208:118161. https://doi.org/10.1016/j.eswa.2022.118161.

11. Qu W, Chui CK, Deng GT, Qian T. Sparse representation of approximation to identity. Anal Appl 2022;20(4):815 – 37. https://doi.org/10.1142/S0219530521500251.

12. Qian T, Zhang Y, Liu WQ, Qu W. Adaptive Fourier decomposition-type sparse representations versus the Karhunen-Loève expansion for decomposing stochastic processes. Math Methods Appl Sci 2023;46(13):14007 – 25. https://doi.org/10.1002/mma.9301.

13. Lu GB, Yang ZF, Qu W, Qian T, Liu ZG, He W, et al. Daily fluctuations in COVID-19 infection rates under Tokyo's epidemic prevention measures–new evidence from adaptive Fourier decomposition. Front Public Health 2023;11:1245572. https://doi.org/10.3389/fpubh.2023.1245572.

14. Qian T, Zhang LM, Li ZX. Algorithm of adaptive fourier decomposition. IEEE Trans Signal Process, 2011;59(12):5899 – 906. https://doi.org/10.1109/TSP.2011.2168520.

15. Qian T, Wang YB. Adaptive Fourier series – a variation of greedy algorithm. Adv Comput Math 2011;34(3):279 – 93. https://doi.org/10.1007/s10444-010-9153-4.

16. Qian T, Wang JZ, Mai WX. An enhancement algorithm for cyclic adaptive fourier decomposition. Appl Comput Harmon Anal 2019;47 (2):516 – 25. https://doi.org/10.1016/j.acha.2019.01.003.

17. Qian T. Two-dimensional adaptive fourier decomposition. Math Methods Appl Sci 2016;39(10):2431 – 48. https://doi.org/10.1002/mma.3649.

18. Qian T. Sparse representations of random signals. Math Methods Appl Sci 2022;45(8):4210 – 30. https://doi.org/10.1002/mma.8033.

19. Hon C, Liu ZG, Qian T, Qu W, Zhao JM. Trends by adaptive fourier decomposition and application in prediction. Int J Wavelets Multiresolut Inf Process. http://dx.doi.org/10.1142/S0219691324500140.

20. Qu W, Qian T, Deng GT. A stochastic sparse representation: *n*-best approximation to random signals and computation. Appl Comput Harmon Anal 2021;55:185 – 98. https://doi.org/10.1016/j.acha.2021.05.003.

21. Pearson K. VII. Note on regression and inheritance in the case of two parents. Proc Roy Soc London 1895;58(347-352):240 – 2. https://doi.org/10.1098/rspl.1895.0041.

22. Tartof SY, Slezak JM, Fischer H, Hong V, Ackerson BK, Ranasinghe ON, et al. Effectiveness of mRNA BNT162b2 COVID-19 vaccine up to 6 months in a large integrated health system in the USA: a retrospective cohort study. Lancet 2021;398(10309):1407 – 16. https://doi.org/10.1016/S0140-6736(21)02183-8.

23. Ghosh A, Nundy S, Ghosh S, Mallick TK. Study of COVID-19 pandemic in London (UK) from urban context. Cities 2020;106:102928. https://doi.org/10.1016/j.cities.2020.102928.

24. Jarvis CI, Van Zandvoort K, Gimma A, Prem K, CMMID COVID-19 working group, Klepac P, et al. Quantifying the impact of physical distance measures on the transmission of COVID-19 in the UK. BMC Med 2020;18(1):124. https://doi.org/10.1186/s12916-020-01597-8.

SUPPLEMENTARY MATERIAL

METHOD

Adaptive Fourier Decomposition (AFD)

AFD features an advanced algorithm optimized for processing discrete time signals by examining their energy distribution. It effectively breaks down a signal into a series of orthogonal components that each have strictly non-negative analytic phase derivatives. These components are arranged by energy level from highest to lowest, supported by a rigorous mathematical framework (*1–6*). The main advantages of AFD include its adaptive generation of basis tailored to the input signal, enabling efficient decomposition, and its ability to adjust the frequency resolution dynamically, thus improving signal processing performance. A critical advantage of AFD over traditional signal processing methods is its distinctive approach to signal decomposition based on energy distribution. This characteristic is particularly beneficial for separating signals with overlapping frequencies, distinguishing AFD from other decomposition techniques (*7–16*).

In the Takenaka-Malmquist system, $\{B_k\}_{k=1}^{\infty}$, is used as the basic element in the calculation of AFD where

$$B_k(z) = \frac{\sqrt{1-|a_k|^2}}{1-\bar{a}_k z} \prod_{j=1}^{k-1} \frac{z-a_j}{1-\bar{a}_j z}, \tag{3}$$

$z = e^{jt}, a_k \in \text{Din} C, k = 1, 2, \cdots$, with C representing the complex plane (Equation 3). For the cause that the characteristics of $B_k(z)$ are related to a_k, the main objective in AFD is to identify specific arrays $\{a_1, a_2, \cdots, a_k\}$, that allow for the decomposition of components, each consisting solely of phase derivatives. This approach results in a high decomposition efficiency with significant physical implications.

All individual components are sequentially extracted from high-energy mode to low-energy mode in the AFD algorithm. To easily determine the energy relationship, the remainder $F_k's$ is reduced and $H_{k-1}'s$ is defined along with their corresponding standard remainder (*7*):

$$F_k(z) = H_{k-1}(z) \prod_{s=1}^{k-1} \frac{1-\bar{a}_s z}{z-a_s}. \tag{4}$$

Therefore, F(z) can be represented by the simplified remainder $F_k's$:

$$F(z) = \sum_{k=1}^{K} \langle F_k, e_{\{a_k\}} \rangle B_k(z) + F_{K+1}(z) \prod_{k=1}^{K} \frac{z-a_k}{1-\bar{a}_k z} \tag{5}$$

The $e_{\{a_k\}}(z)$ is called the evaluator at a_k, which creates a dictionary of the Hardy space $H^2(D)$ (*3*):

$$e_{\{a_k\}}(z) = \frac{\sqrt{1-|a_k|^2}}{1-\bar{a}_k z}. \tag{6}$$

The complex Hardy space in the unit circle D is defined as follows:

$$H^2(D) = \left\{ f: D \to \mathbb{C} : f \text{ is holomorphic, and } ||f||_2^2 \triangleq \sup_{1>r\geq0} \int_0^{2\pi} |f(rz)|^2 dz < \infty \right\}.$$

In compliance with Equation 5, the energy of F(z) can be calculated as (*1*).

$$||F(z)||^2 = \sum_{k=1}^{K} |\langle F_k, e_{\{a_k\}} \rangle|^2 + ||G_{K+1}(z)||^2. \tag{7}$$

To minimize the energy of the standard remainder $||F_{K+1}(z)||^2$, the maximum projection principle outlined in Equation 8 is utilized to find a_k that can yield the maximum $|\langle F_k, e_{\{a_k\}} \rangle|^2$ for each step in (*7*).

$$a_k = \text{argmax}\left\{ |\langle F_k, e_{\{a_k\}} \rangle|^2 : a_k \in D \right\} \tag{8}$$

Enhancement of Construction Components via AFD

We constructed new components based on the decomposition results (Equation 9):

$$D_p(q) = \sum_{m=pq-q+1}^{pq} C_m B_m(z),$$ (9)

$$where z = e^{jt},$$

$$C_m = \langle F_m, e_{\{a_m\}} \rangle,$$

$$and B_m(z) = \frac{\sqrt{1-|a_m|^2}}{1-\bar{a}_m z} \prod_{k=1}^{m-1} \frac{z-a_k}{1-\bar{a}_k z}.$$

The original signal was obtained by constructing all of the components (Equtation 10).

$$W_q = \sum_{p=1}^{r} D_p(q)$$ (10)

Figure 2 illustrates the decomposition of original data into eight primary components using AFD. These components were reassembled into eight new components for the scenario where q=1, as described in Equation 9. As shown in column A of Figure 3, Comp1 corresponds to the case where p=1 and q=1, progressing sequentially to Comp8, which corresponds to p=8 and q=1. By overlaying these eight reconstructed components in accordance with Equation 10, the original signal was successfully restored.

In the second stage of AFD, the initial dataset was decomposed into 16 primary components via AFD. Subsequently, these components were reorganized into eight new components, adhering to q=2 as specified in Equation 9. As depicted in column B of Figure 3, components Comp1 through Comp8 correspond to parameters ranging from p=1, q=2 to p=8, q=2, respectively. By superimposing these eight new components according to Equation 10, the original signal was successfully reconstructed.

In the third application of AFD, the original dataset was segmented into 24 distinct components using the AFD method. Subsequently, these components were reorganized into eight new components under the condition where q=3 as outlined in Equation 9. As depicted in column C of Figure 3, components Comp1 through Comp8 were sequentially assigned to represent values from p=1 and q=3 to p=8 and q=3, respectively. By overlaying these eight reconstructed components in accordance with Equation 10, the original signal was successfully restored.

Figure 3 horizontally displays columns labeled A to C, each illustrating the progression from the basic AFD to the enhanced third-order AFD construction components. These columns distinctly represent fluctuations in the number of COVID-19 cases. Vertically, the eight rows are arranged from the lowest to the highest frequency components, reflecting temporal changes in case counts throughout the study period and providing a detailed analysis of the pandemic's progression.

Pearson Correlation Coefficient

The correlation analysis is an essential statistical tool used to determine the strength and direction of a linear relationship between two quantitative variables. This relationship is quantified by the correlation coefficient, denoted as "r", which ranges from –1 to 1. A value of –1 indicates a perfect negative linear correlation, 1 indicates a perfect positive linear correlation, and 0 signifies no linear correlation (15). Additionally, this analysis calculates a P value to assess the probability of obtaining the observed coefficient, r, assuming that no actual correlation exists in the population. A small P value suggests that the observed correlation is statistically significant and not due to random chance (16). Understanding the Pearson correlation coefficient is crucial for interpreting the linear associations between variables.

The Pearson correlation coefficient r between two variables x and y is defined as:

$$r = \frac{\sum_{i=1}^{n}\left(x_i - \bar{x}\right)\left(y_i - \bar{y}\right)}{\sqrt{\sum_{i=1}^{n}\left(x_i - \bar{x}\right)^2}\sqrt{\sum_{i=1}^{n}\left(y_i - \bar{y}\right)^2}}$$ (11)

where x_i and y_i are the ith data points; $\bar{x}$ and $\bar{y}$ are the means of X and Y, respectively; and n is the number of data points.

REFERENCES

1. Qian T. Intrinsic mono-component decomposition of functions: an advance of Fourier theory. Math Methods Appl Sci 2010;33(7):880 – 91. https://doi.org/10.1002/mma.1214.
2. Qian T. Cyclic AFD algorithm for the best rational approximation. Math Methods Appl Sci 2014;37(6):846 – 59. https://doi.org/10.1002/mma.2843.
3. Qian T, Wang YB. Adaptive Fourier series – a variation of greedy algorithm. Adv Comput Math 2011;34(3):279 – 93. https://doi.org/10.1007/s10444-010-9153-4.
4. Qian T, Wang JZ, Mai WX. An enhancement algorithm for cyclic adaptive fourier decomposition. Appl Comput Harmon Anal 2019;47(2):516 – 25. https://doi.org/10.1016/j.acha.2019.01.003.
5. Qian T. Two-dimensional adaptive fourier decomposition. Math Methods Appl Sci 2016;39(10):2431 – 48. https://doi.org/10.1002/mma.3649.
6. Qian T. Sparse representations of random signals. Math Methods Appl Sci 2022;45(8):4210 – 30. https://doi.org/10.1002/mma.8033.
7. Hon C, Liu ZG, Qian T, Qu W, Zhao JM. Trends by adaptive fourier decomposition and application in prediction. Int J Wavelets Multiresolut Inf Process. http://dx.doi.org/10.1142/S0219691324500140.
8. Qu W, Qian T, Deng GT. A stochastic sparse representation: n-best approximation to random signals and computation. Appl Comput Harmon Anal 2021;55:185 – 98. https://doi.org/10.1016/j.acha.2021.05.003.
9. Qu W, Chui CK, Deng GT, Qian T. Sparse representation of approximation to identity. Anal Appl 2022;20(4):815 – 37. https://doi.org/10.1142/S0219530521500251.
10. Qian T, Zhang Y, Liu WQ, Qu W. Adaptive Fourier decomposition-type sparse representations versus the Karhunen-Loève expansion for decomposing stochastic processes. Math Methods Appl Sci 2023;46(13):14007 – 25. https://doi.org/10.1002/mma.9301.
11. Dai L, Zhang LM. A joint spatiotemporal video compression based on stochastic adaptive fourier decomposition. IEEE Signal Process Lett 2022;29:1531 – 5. https://doi.org/10.1109/LSP.2022.3187917.
12. Saâdaoui F, Mefteh-Wali S, Ben Jabeur S. Multiresolutional statistical machine learning for testing interdependence of power markets: a Variational Mode Decomposition-based approach. Expert Syst Appl 2022;208:118161. https://doi.org/10.1016/j.eswa.2022.118161.
13. Wang Z, Wan F, Wong CM, Zhang LM. Adaptive Fourier decomposition based ECG denoising. Comput Biol Med 2016;77:195 – 205. https://doi.org/10.1016/j.compbiomed.2016.08.013.
14. Wang Z, Nuno da Cruz J, Wan F. Adaptive Fourier decomposition approach for lung-heart sound separation. In: Proceedings of 2015 IEEE international conference on computational intelligence and virtual environments for measurement systems and applications. Shenzhen, China: IEEE. 2015. http://dx.doi.org/10.1109/CIVEMSA.2015.7158631.
15. Pearson K. VII. Note on regression and inheritance in the case of two parents. Proc Roy Soc London 1895;58(347-352):240 – 2. https://doi.org/10.1098/rspl.1895.0041.
16. Field A. Discovering statistics using IBM SPSS statistics. SAGE. 2013. https://us.sagepub.com/en-us/nam/discovering-statistics-using-ibm-spss-statistics/book260423.